*32nd URSI GASS, Montreal, 19–26 August 2017*

# Spectral Analysis of Finite Difference Models of Open Structures in Time and Frequency Domain

Philipp Jorkowski, Lilli Kuen, and Rolf Schuhmann*
Technische Universität Berlin, Theoretische Elektrotechnik, EN-2, 10587 Berlin, Germany, http://www.tet.tu-berlin.de

## Abstract

We present an analysis of extended, FDTD-like methods which is based on the eigenvalues of the iteration matrix. For a stable update scheme these eigenvalues must lie within the unit circle, and this kind of analysis is applied to systems with radiation losses. For small models, it is possible to compute the eigenvalues numerically and to compare them to the spectrum of the corresponding time-continuous formulation. This allows to assess the accuracy and stability properties of different implementation variants.

## 1 Introduction

The spectral properties of the system matrix of Finite Difference or Finite Integration (FIT) models can be used to analyze important issues such as the stability, the conservation of discrete energy, the applicability of specials solvers, or the consistency of extended spatial operators. Without conductivity losses and using closed boundary conditions, all eigenvalues of the time-continuous formulation (frequency domain, FD, or time domain, TD, before time-stepping being applied) can be correlated to real-valued eigenfrequencies $\omega_i$. This can be expressed in FD and in the language of the Finite Integration Technique [1] as

$$\begin{pmatrix} \mathbf{C} & s\mathbf{M}_\mu \\ -s\mathbf{M}_\varepsilon & \mathbf{C}^T \end{pmatrix} \begin{pmatrix} \widehat{\mathbf{e}} \\ \widehat{\mathbf{h}} \end{pmatrix} = \begin{pmatrix} 0 \\ 0 \end{pmatrix}, \tag{1}$$

$$\text{or} \quad \mathbf{C}^T \mathbf{M}_\mu^{-1} \mathbf{C}\, \widehat{\mathbf{e}} + s^2 \mathbf{M}_\varepsilon\, \widehat{\mathbf{e}} = 0, \tag{2}$$

with the frequency parameter $s = j\omega$, the curl-matrix $\mathbf{C}$, the (diagonal) material matrices $\mathbf{M}_\mu$ and $\mathbf{M}_\varepsilon$, and the magnetic and electric grid voltages $\widehat{\mathbf{h}}$, $\widehat{\mathbf{e}}$, respectively. Note that (1) and (2) not only neglect exciting currents ($\widehat{\widehat{\mathbf{j}}}$=0) and conductivity losses ($\mathbf{M}_\sigma = 0$), but also implicitly impose closed boundary conditions if used in this simplest form.

For a TD implementation using the leapfrog time stepping scheme, we apply central difference formulas for the time derivatives (factor $s$), leading to the update equations

$$\begin{aligned} \widehat{\mathbf{e}}^{n+\frac{1}{2}} &= \widehat{\mathbf{e}}^{n-\frac{1}{2}} + \Delta t \mathbf{M}_\varepsilon^{-1} \mathbf{C}^T \widehat{\mathbf{h}}^n, \\ \widehat{\mathbf{h}}^{n+1} &= \widehat{\mathbf{h}}^{n} \quad - \Delta t \mathbf{M}_\mu^{-1} \mathbf{C} \widehat{\mathbf{e}}^{n+\frac{1}{2}}, \end{aligned}$$

$$\text{or} \quad \begin{pmatrix} \widehat{\mathbf{e}} \\ \widehat{\mathbf{h}} \end{pmatrix}^{new} = \underbrace{\begin{pmatrix} \mathbf{I} & \Delta t \mathbf{A}_{12} \\ -\Delta t \mathbf{A}_{21} & \mathbf{I} - \Delta t^2 \mathbf{A}_{21}\mathbf{A}_{12} \end{pmatrix}}_{\mathbf{G}(\Delta t)} \begin{pmatrix} \widehat{\mathbf{e}} \\ \widehat{\mathbf{h}} \end{pmatrix}^{old}, \tag{3}$$

with $\mathbf{A}_{12} = \mathbf{M}_\varepsilon^{-1}\mathbf{C}^T$, $\mathbf{A}_{21} = \mathbf{M}_\mu^{-1}\mathbf{C}$. The so-called iteration matrix $\mathbf{G}(\Delta t)$ has transformed eigenvalues $\underline{\lambda}_{TD} = \exp(j\varphi)$ which can be interpreted as a phase advance $\varphi = \hat{\omega}\Delta t$ per time step. Herein, $\hat{\omega}$ can be identified as the approximated eigenfrequency according to the numerical dispersion relation. (For standard textbook results on the leapfrog method cf., e.g., [1, 2]) Note that $\mathbf{G}$ is always a real-valued matrix with pairs of conjugate complex eigensolutions.

It is well-known that the leapfrog scheme (3) with a time step below the Courant limit (CFL) only has time-domain eigenvalues $\underline{\lambda}_{TD}$ on the unit circle, corresponding to real-valued eigenfrequencies $\hat{\omega}$. This is equivalent to numerical stability. Situation changes, however, with the presence of losses: Obviously, the eigenfrequencies become complex numbers $\underline{\hat{\omega}}$, where the non-negative imaginary part defines the damping coefficient of free oscillations. In the same manner, the time-domain eigenvalues $\underline{\lambda}_{TD}$ are shifted to magnitudes $|\underline{\lambda}_i| \leq 1$ on or within the unit circle. However, the algebraic analysis becomes more involved, since the losses can be correlated to a number of different expressions in the wave equation: first order derivatives in the wave equation for conduction losses, higher order terms for dispersive materials, or even more complicated formulations for absorbing boundary conditions. The same holds in FD, where one obtains polynomial or generally non-linear dependencies of the system matrix from the frequency $s$.

## 2 PML formulation

We concentrate here on radiation losses, i.e. we analyze simple setups without conductivity, but with at least one boundary allowing radiation, realized by a Perfectly Matched Layer (PML) boundary condition [3, 4]. The PML consists of a couple of additional grid layers containing an artificial material with a specific frequency dependence. It can be formulated in FD as

$$(\mathbf{I} + \frac{1}{s}\sigma_n)\mathbf{C}\widehat{\mathbf{e}} = -s(\mathbf{I} + \frac{1}{s}\sigma_{t1} + \frac{1}{s^2}\sigma_{t2})\mathbf{M}_\mu \widehat{\mathbf{h}}, \tag{4}$$

$$(\mathbf{I} + \frac{1}{s}\kappa_n)\mathbf{C}^T\widehat{\mathbf{h}} = s(\mathbf{I} + \frac{1}{s}\kappa_{t1} + \frac{1}{s^2}\kappa_{t2})\mathbf{M}_\varepsilon \widehat{\mathbf{e}}. \tag{5}$$

Herein, the matrices $\kappa_{t1}$, $\kappa_{t2}$, $\sigma_{t1}$, $\sigma_{t2}$ are electric and magnetic losses for the tangential coefficients in the PML, respectively. $\kappa_n$ and $\sigma_n$ contain the losses for normal coefficients and have an inverse $s$-dependency. For simplicity, we

only use a single PML for the $z_{max}$-boundary of the computational domain, and thus $\sigma_{t2} = \kappa_{t2} = 0$. Note that there may be some implementation options in the spatial discretization of these operations, e.g. concerning the allocation of the loss profiles on the grid, which are not discussed here.

The modified eigenvalue problem in FD reads

$$\underbrace{\begin{pmatrix} (s\mathbf{I}+\sigma_n)\mathbf{C} & (s^2\mathbf{I}+s\sigma_{t1})\mathbf{M}_\mu \\ -(s^2\mathbf{I}+s\kappa_{t1})\mathbf{M}_\varepsilon & (s\mathbf{I}+\kappa_n)\mathbf{C}^T \end{pmatrix}}_{\mathbf{T}(s)} \underbrace{\begin{pmatrix} \widehat{\mathbf{e}} \\ \widehat{\mathbf{h}} \end{pmatrix}}_{\mathbf{v}} = \begin{pmatrix} 0 \\ 0 \end{pmatrix}. \quad (6)$$

Due to the frequency dependence of the PML coefficients, this eigenvalue problem is non-linear, in this case polynomial (quadratic) w.r.t the eigenvalues $s$.

In TD, several extensions of the standard leapfrog formulas are necessary. First, the $s^{-1}$ expressions translate into integrations which are realized by additional state variables

$$\phi(t) = \int_0^t \widehat{\mathbf{e}}(\tau)\mathrm{d}\tau, \qquad \psi(t) = \int_0^t \widehat{\mathbf{h}}(\tau)\mathrm{d}\tau. \quad (7)$$

Concerning the discretization in time, there is some reasoning to allocate these quantities either on full or on half time steps of the time axis, respectively, and it is hard to assess which of these variants is to be preferred. Second, the loss terms have to be time-discretized, and again, the allocation of quantities on the time axis is an issue.

As one option we use here the following assignments,

$$\phi(t) \to \phi^{n+\frac{1}{2}} \qquad \psi(t) \to \psi^n \quad (8)$$

$$\widehat{\mathbf{e}}^n \approx \frac{\widehat{\mathbf{e}}^{n+\frac{1}{2}} + \widehat{\mathbf{e}}^{n-\frac{1}{2}}}{2} \qquad \widehat{\mathbf{h}}^{n+\frac{1}{2}} \approx \frac{\widehat{\mathbf{h}}^n + \widehat{\mathbf{h}}^{n+1}}{2} \quad (9)$$

where the second line defines the implementation of magnetic and electric losses (PML coefficients $\sigma_{t1}$ and $\kappa_{t1}$).

This directly leads to an extended update scheme:

$$\begin{aligned}
\widehat{\mathbf{e}}^{n+\frac{1}{2}} &= \mathbf{M}_\varepsilon^{-1}(\mathbf{I}+\frac{\Delta t}{2}\kappa_{t1})^{-1} \\
&\quad \left[(\mathbf{I}-\frac{\Delta t}{2}\kappa_{t1})\mathbf{M}_\varepsilon \widehat{\mathbf{e}}^{n-\frac{1}{2}} + \Delta t(\mathbf{C}^T\widehat{\mathbf{h}}^n + \kappa_n \mathbf{C}^T\psi^n)\right] \\
\phi^{n+\frac{1}{2}} &= \phi^{n-\frac{1}{2}} + \Delta t\, \widehat{\mathbf{e}}^{n+\frac{1}{2}} \\
\widehat{\mathbf{h}}^{n+1} &= \mathbf{M}_\mu^{-1}(\mathbf{I}+\frac{\Delta t}{2}\sigma_{t1})^{-1} \\
&\quad \left[(\mathbf{I}-\frac{\Delta t}{2}\sigma_{t1})\mathbf{M}_\mu \widehat{\mathbf{h}}^n - \Delta t(\mathbf{C}\widehat{\mathbf{e}}^{n+\frac{1}{2}} + \sigma_n \mathbf{C}\phi^{n+\frac{1}{2}})\right] \\
\psi^{n+1} &= \psi^n + \Delta t\, \widehat{\mathbf{h}}^{n+1} \quad (10)
\end{aligned}$$

Note that the inverse matrices are trivial to build since all material matrices are diagonal within FIT. An alternative variant is to use so-called exponential time-stepping, i.e. to solve a simplified form of the corresponding ODE analytically in order to obtain modified update equations for $\widehat{\mathbf{e}}^{n+\frac{1}{2}}$ and $\widehat{\mathbf{h}}^{n+1}$, respectively. The formulas are not repeated here. Although both schemes are convergent for $\Delta t \to 0$, they have slightly different properties for finite $\Delta t > 0$.

As a consequence, the iteration matrix $\mathbf{G}$ has to be reformulated in terms of an increased number of unknowns ($\widehat{\mathbf{e}}$, $\widehat{\mathbf{h}}$, as well as $\phi$ and $\psi$ in the PML region) and the more complicated connections between those. Although it is possible in this case to find a closed-form notation of $\mathbf{G}$ from (10), we use a different approach which is directly based on the implementation of the update equations in our code: We artificially define unit vectors of the complete dof-vector $[\widehat{\mathbf{e}};\widehat{\mathbf{h}};\phi;\psi]$, apply one time step of the update cycle, and assemble the (combined) result vector as one column of $\mathbf{G}$. Of course, this procedure is only feasible for small or medium-size models. However, its main advantage is its general applicability also for more involved update schemes, and one can be sure that the *actually used* update scheme will finally be represented by $\mathbf{G}$ – including any additional 'tricks' as well as possible bugs in the implementation. Finally the eigenvalues of $\mathbf{T}(s)$ and $\mathbf{G}(\Delta t)$ can be solved numerically.

# 3 Numerical Evaluation

## 3.1 Non-linear Eigensolver

The quadratic eigenvalue problem (QEVP) in (6) with the matrix $\mathbf{T}(s)$ can be rewritten as

$$(\mathbf{A}_2 s^2 + \mathbf{A}_1 s + \mathbf{A}_0)\mathbf{v} = 0. \quad (11)$$

For a numerical evaluation of this equation, a couple of standard and more involved techniques exist. One of them is the general nonlinear eigensolver described in [5] which has already been tested for a similar formulation in [6]. Alternatively, due to the implementation of this project in Matlab [7], the Matlab internal polynomial eigensolver `polyeig` is used. It applies a linearization of the QEPV, doubling the effective matrix size. In both cases, the quality of the results is checked by calculating residuals.

Note that the matrices in (11) require to be scaled before handing them over to a solver: For a common FD analysis with expected eigenvalues $s = j2\pi f$ in the GHz area, the factor of $10^{20}$ between $\mathbf{A}_2$ and $\mathbf{A}_0$ may cause severe numerical problems. Nevertheless, the solvers can only be applied for problems with small matrix dimensions.

## 3.2 Setup

Our validation example is chosen to be simple enough to enable a numerical analysis of the full spectra of the system matrix and the iteration matrix, but on the other hand contains some of the typical properties to be expected in the context of PML-bounded resonators.

Fig. 1 shows a circular hollow waveguide with radius $R = 1$ and length $L = 8$ (all in SI units), where the section $-1 <$

$z < 1$ contains a dielectric material with $\varepsilon_r = 16$. This dielectric contrast produces the resonances, but only eigensolutions above the cut-off frequency of the corresponding transversal waveguide-mode can radiate through the open waveguide. Moreover, it is well-known that the performance of standard PML breaks down for waveguide modes near their cutoff-frequency, which may be one source for irregular behavior and even instabilities in TD.

One azimuthal slice of the model is discretized spatially by a two-dimensional body-of-revolution grid in $\rho, z$-coordinates with $N = N_\rho \times N_z$ mesh cells and a symmetry-boundary (perfect magnetic conductor, PMC) at $z = 0$. At the upper boundary $N_{PML}$ layers of a PML are added. The azimuthal order is set to $m = 1$. Several levels of discretization, starting with a very coarse grid, have been tested.

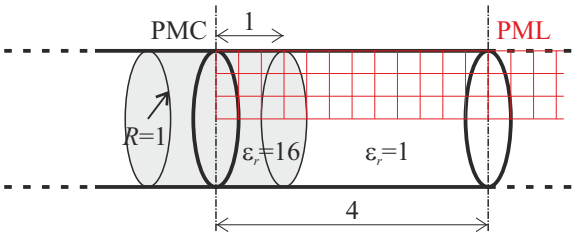


**Figure 1.** Simple model of a circular waveguide resonator with a high dielectric contrast to obtain resonances. Spatial discretization by a two-dimensional mesh (in red).

Since the structure is longitudinally homogenous, all eigenmodes can be interpreted as propagating or attenuated waveguide modes in the two sections (quasi-1D behavior). Moreover, the exact (*discrete*) cutoff-frequency of each transversal mode can easily be calculated. This enables us to identify each eigensolution of the full structure, and even to calculate reference solutions analytically [6].

## 3.3 Spectral Analysis

Fig. 2 shows the spectrum of the time-continuous formulation (6) for the smallest grid size $N_\rho = 3$, $N_z = 5$, and $N_{PML} = 3$. As expected, all eigenvalues appear as pairs with $\pm\Re\{\underline{\omega}_i\}$, and their non-negative imaginary parts identify them as stable solutions of this time-continuous system.

The following classes of solutions can be identified:
$\rightarrow$ Non-damped modes on the real axis: typically eigenmodes where the transversal pattern is defined by a waveguide mode below cutoff, with exponential decay for $z > 1$ and no power transport through the PML.
$\rightarrow$ Damped modes with small imaginary parts: starting from the cutoff-frequency of a specific waveguide mode, these eigenvalues follow some path with increasing losses.
$\rightarrow$ Modes with larger imaginary part: non-physical 'PML-modes' with fields primarily in the PML region.
$\rightarrow$ Static modes (zero eigenvalues): well-known from the wave-equation.

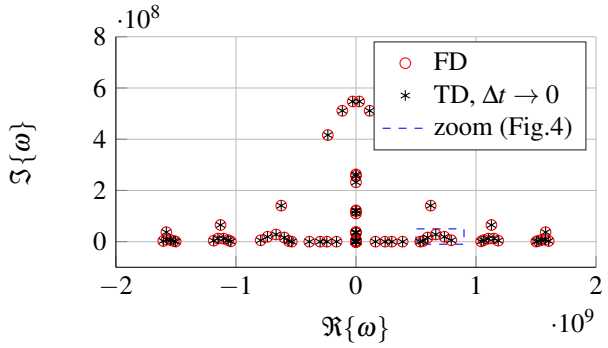


**Figure 2.** Full spectrum of the non-linear eigenvalue formulation (6) in FD and the transformed results from TD with $\Delta t \rightarrow 0$. Several classes of solutions are visible.

Both the PML-modes and the static modes are obviously stable, with a imaginary part equal to or well above zero. However, their properties within the PML is not well understood so far, and stability may be hard to prove for the general case. A refinement of the grid does not imply any qualitative changes.

Although this simple spectrum is only an exemplary representative and may considerably change for more general examples, it allows identifying candidates for possible stability properties of a TD solution:
$\rightarrow$ all modes with small or vanishing imaginary part, and
$\rightarrow$ a non-vanishing part of the fields in or near the PML (since we know that standard leapfrog without PML and other extensions is always stable), and
$\rightarrow$ maybe an eigenfrequency near to one of the cutoff-frequencies in the waveguide.
The stability of some of these modes is not clear a priori, since the complicated nature of the spatially discretized, non-standard material model of the PML is difficult to analyze. Additionally, even if stable in the time-continuous regime, the additional approximation due to the finite time step may shift some eigenvalues to the 'wrong' half of the complex domain. Such a behavior has been occasionally observed using the exponential time-stepping which will be reported in detail in a subsequent paper.

Here only the eigenvalues of the TD iteration matrix derived from (10) are shown, see Fig. 3. The time step $\Delta t$ is chosen close to leapfrog's CFL limit $\Delta t_{max}$. This means that some of the oscillations would be poorly sampled in time, (the CFL limit is related to the sampling limit w.r.t. the transformed eigenfrequency), and their deviation to the FD solution is expected to be large. Note that this sampling rate is different for each mode: the smallest eigenfrequencies are typically well-sampled, but of course the stability criterion must be fulfilled for *all* modes in the spectrum.

After scaling the eigenvalues by $\hat{\underline{\omega}} = \ln(\underline{\lambda}_{TD})/(j\Delta t)$, they can be directly compared to the eigenfrequencies from the FD spectrum. As expected, the spectra of the TD- and FD-formulation always show the same structure, and the TD-

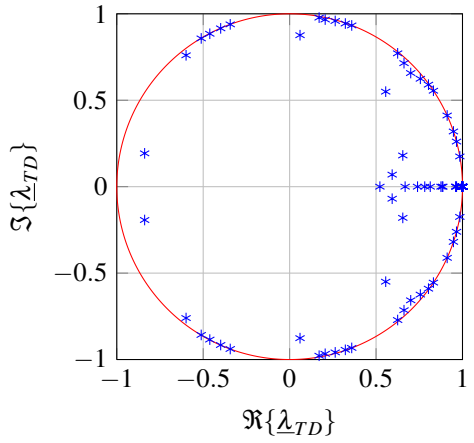


**Figure 3.** Spectrum of the TD iteration matrix with PML.

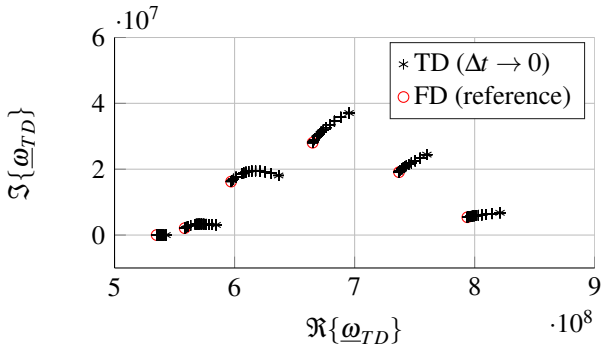


**Figure 4.** Zoomed part of the spectrum of Fig. 2 with convergence of TD eigenvalues for $\Delta t \to 0$.

eigenvalues converge towards the FD values for a decreasing time step ($\Delta t \to 0$, included in Fig. 2). The convergence in the complex plane is visualized for some modes in the zoomed plot in Fig. 4. The deviations from the FD solutions are large enough to be a significant issue for stability.

Finally, the convergence curves for two modes are shown in Fig. 5. The 2nd-order curves for larger time steps – the expected behavior for standard leapfrog due to the central difference expressions involved – are deteriorated for smaller $\Delta t$. The reason for this is the allocation of the additional quantities $\phi$ and $\psi$ and the non-central realization of (7) in (10). How this may be avoided in spite of the complicated nature of the PML will be subject of further research.

## 4 Conclusions

The comparison of eigenmodes from the frequency domain system matrix and the time domain iteration matrix is a powerful methodology to understand some properties of time-stepping schemes, especially their possible instability issues in the context of PML. In frequency domain, the solution of a polynomial eigenvalue problem is required, and in time domain the system has to be enlarged by the additional degrees of freedom used within the update scheme.

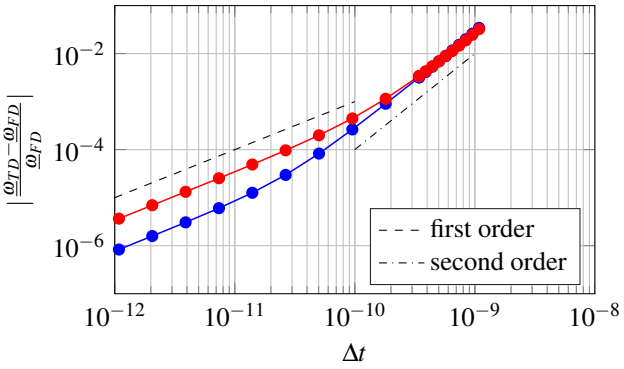


**Figure 5.** Convergence of two (arbitrarily chosen) TD eigenvalues towards the FD reference solution w.r.t $\Delta t \to 0$.

Although the spectra can only be computed for small, academic examples, the influence of the additional approximation of the time discretization can be studied for typical situations. In this paper we mainly describe the idea of this approach, but also have shown some preliminary results for a certain class of radiating resonant structures. We have discussed several classes of eigenmodes which are prone to instabilities, e.g. due to the limited performance of PML near cutoff phenomena, or the non-physical nature of special 'PML-modes'. Their detailed investigation in terms of different time-discretization methods will be subject of further research. An additional benefit of this approach is a deeper understanding of the spectral properties of discretized, resonant (or non-resonant) electromagnetic structures.

## References

[1] T. Weiland, "Time Domain Electromagnetic Field Computation with Finite Difference Methods," *Int. Journal of Num. Modelling*, **9**, 4, 1996, pp. 295–319.

[2] A. Taflove, S.C. Hagness, "Computational Electrodynamics: The Finite-Difference Time-Domain Method," 2nd ed., Artech House, 2000.

[3] J.P. Berenger, "Perfectly Matched Layer (PML) for Computational Electromagnetics," *Synthesis Lectures on Computational Electromagnetics*, Morgan & Claypool Publishers, 2007.

[4] L. Zhao, A. C. Cangellaris, "GT-PML: Generalized Theory of Perfectly Matched Layers and its Application to the Reflectionless Truncation of Finite-Difference Time-Domain Grids", *IEEE Trans. MTT*, **44**, 12, 1996, pp. 2555–2563.

[5] W.-J. Beyn, "An Integral Method for Solving Nonlinear Eigenvalue Problems," *Linear Algebra and its Applications*, **436**, 10, 2012, pp. 3839–3863.

[6] P. Jorkowski, "Nichtlinearer Eigenwertlöser zur Simulation von wellenleitergekoppelten elektromagnetischen Resonatoren," MSc Thesis, TU Berlin, 2015.

[7] MATLAB, The MathWorks Inc., Natick, MA, 2017.